Implementation of the multiconfiguration time-dependent Hatree-Fock method for general molecules on a multi-resolution Cartesian grid

Ryohto Sawada,[1,2] Takeshi Sato,[2,3] and Kenichi L. Ishikawa[2,3]

[1]*Department of Applied Physics, Graduate School of Engineering, The University of Tokyo, 7-3-1 Hongo, Bunkyo-ku, Tokyo 113-8656, Japan*
[2]*Photon Science Center, Graduate School of Engineering, The University of Tokyo, 7-3-1 Hongo, Bunkyo-ku, Tokyo 113-8656, Japan*
[3]*Department of Nuclear Engineering and Management, Graduate School of Engineering, The University of Tokyo, 7-3-1 Hongo, Bunkyo-ku, Tokyo 113-8656, Japan*

(Dated: January 8, 2016)

We report a three-dimensional numerical implementation of multiconfiguration time-dependent Hartree-Fock (MCTDHF) based on a multi-resolution Cartesian grid, with no need to assume any symmetry of molecular structure. We successfully compute high-harmonic generation (HHG) of H_2 and H_2O. The present implementation will open a way to the first-principle theoretical study of intense-field and attosecond-pulse induced ultrafast phenomena in general molecules.

PACS numbers: 33.80.Rv, 31.15.A-, 42.65.Ky,

I. INTRODUCTION

The dynamics of atoms and molecules under intense (typically $\gtrsim 10^{14}\,\mathrm{W/cm^2}$) laser pulses is of great interest in a variety of fields such as attosecond science and high-field physics [1–3], with a goal to directly measure and manipulate electronic motion. Numerical simulations of such electron dynamics are a challenging task [4]. Direct solution of the time-dependent Schrödinger equation (TDSE) cannot be applied beyond He, H_2, and Li, due to a prohibitive computational cost. Thus, one of major recent directions attracting increasing interest is the multiconfiguration self-consistent-field (MCSCF) approach, which expresses the total wave function $\Psi(t)$ as a superposition [5–9]

$$|\Psi(t)\rangle = \sum_J c_J(t)|J\rangle, \tag{1}$$

of Slater determinants $|I\rangle$ built from spin orbitals $|\phi_{(i,\sigma)}\rangle = |\phi_i\rangle \otimes |\sigma\rangle$, where $\{\phi_i\}$ and $\sigma \in \{\alpha, \beta\}$ denote one-electron spatial orbital functions and spin eigenfunctions, respectively. Different variants with this *ansatz* have recently been actively developed [4].

The time-dependent configuration-interaction (TDCI) methods take orbital functions to be time-independent and propagate only CI coefficients $c_I(t)$. Santra *et al.* [10] have implemented its simplest variant, i.e., the time-dependent configuration-interaction singles (TDCIS) method to treat atomic high-field processes. In this method, only up to single-orbital excitation from the Hartree-Fock (HF) ground-state is included. Bauch *el al.* [11] have recently developed TD generalized-active-space CI based on a general CI truncation scheme and discussed its numerical implementation for atoms and diatomic molecules.

In the other class of MCSCF approaches, not only CI coefficients but also orbital functions are varied in time. The multiconfiguration time-dependent Hartree-Fock (MCTDHF) [12, 13] considers all the possible electronic configuration for a given number of spin orbitals. As its flexible generalizations, we have recently formulated the TD complete-active-space self-consistent field (TD-CASSCF) [8] and TD occupation-restricted multiple-active space (TD-ORMAS) [9] methods. The latter is valid for general MCSCF wave functions with arbitrary CI spaces [4, 14] including, e.g., the TD restricted-active-space self-consistent-field (TD-RASSCF) theory developed by Miyagi and Madsen [15]. Numerical implementations of MCTDHF for atoms as well as diatomic molecules have been reported for the calculation of valence and core photoionization cross sections [16]. We have also implemented TD-CASSCF for atoms by expanding orbital functions with spherical harmonics and successfully computed high-harmonic generation and nonsequential double ionization of Be [17].

Practically all the existing implementations are intended for atoms and diatomic molecules, exploiting the underlying symmetries with either the spherical [18–22], cylindrical [23–26], or prolate spheroidal [27–30] coordinates.

In this study, we report a three-dimensional (3D) numerical implementation of MCTDHF based on a multi-resolution Cartesian grid, with no need to assume any symmetry of molecular structure, this can in principle be applied to any molecule. With the use of a multi-resolution finite-element representation of orbital functions, we can fulfill a high degree of refinement near nuclei and, at the same time, a simulation domain large enough to sustain departing electrons. As demonstrations, we successfully compute high-harmonic generation (HHG) from H_2 and H_2O. The present implementation will open a way to the first-principle theoretical study of intense-field and attosecond-pulse induced ultrafast phenomena in general molecules.

This paper is organized as follows. In Sec. II, we briefly

summarize the MCTDHF method. Section III describes the multi-resolution cartesian grid. Section IV explains the numerical procedure that we implement. In Sec. V, we show examples of simulation results for He, H_2, and H_2O. Conclusions are given in Sec. VI. Atomic units are used throughout unless otherwise stated.

II. MCTDHF

In the MCTDHF method [12, 13], the sum in Eq. (1) runs over the complete set of $\binom{M}{N_\alpha}\binom{M}{N_\beta}$ Slater determinants $|J\rangle$ that can be constructed from N_α electrons with spin-projection α, N_β electrons with spin-projection β, and M spatial orbitals. Their spin-projection is consequently restrited to $S_z = (N_\alpha - N_\beta)/2$.

Let us consider a Hamiltonian in the length gauge,

$$H(t) = H_1(t) + H_2, \tag{2}$$

$$H_1(t) = \sum_{i=1}^{N}\left(-\frac{\nabla_i^2}{2} - \sum_a \frac{Z_a}{|\mathbf{x}_i - \mathbf{X}_a|} + \mathbf{x}_i \cdot \mathbf{E}(t)\right), \tag{3}$$

$$H_2 = \sum_{i=1}^{N}\sum_{j=1}^{i-1}\frac{1}{|\mathbf{x}_i - \mathbf{x}_j|}, \tag{4}$$

where $N = N_\alpha + N_\beta$, X_a and Z_a are the charge and position of the a-th atom, respectively, and $\mathbf{E}$(t) is the laser electronic field. One can derive the equations of motion for the CI coefficients $c_J(t)$ and spatial orbital functions $\phi_i(t)$, resorting to the time dependent variational principle [31–33],

$$\delta\left(\int_{t_1}^{t_2}\langle\Psi|H(t) - i\partial_t|\Psi\rangle dt\right) = 0 \tag{5}$$

with additional constraints for uniqueness [12],

$$\langle\phi_j|\phi_k\rangle = \delta_{j,k}, \quad \left\langle\phi_j\middle|\frac{\partial\phi_k}{\partial t}\right\rangle = 0. \tag{6}$$

The equations of motion are,

$$i\dot{c}_J = \sum_K \langle J|H(t)|K\rangle\, c_K, \tag{7}$$

and

$$i|\dot{\phi}_i\rangle = \hat{P}\left(H_1(t)|\phi_i\rangle + \sum_{jklm}(\rho^{-1})_{ij}\rho^{(2)}_{jklm}\hat{g}_{lm}|\phi_k\rangle\right), \tag{8}$$

with,

$$\hat{P} = \hat{\mathbf{1}} - \sum_{j=1}^{M}|\phi_j\rangle\langle\phi_j|, \tag{9}$$

$$\rho_{i,j} = \sum_\sigma\langle\Psi|\hat{a}^\dagger_{i\sigma}\hat{a}_{j\sigma}|\Psi\rangle, \tag{10}$$

$$\rho^{(2)}_{jklm} = \sum_{\sigma\tau}\langle\Psi|\hat{a}^\dagger_{j\sigma}\hat{a}^\dagger_{l\tau}\hat{a}_{m\tau}\hat{a}_{k\sigma}|\Psi\rangle, \tag{11}$$

$$g_{lm}(\mathbf{x}) = \int d\mathbf{x}'\phi^*_l(\mathbf{x}')\frac{1}{|\mathbf{x} - \mathbf{x}'|}\phi_m(\mathbf{x}'), \tag{12}$$

where $\hat{\mathbf{1}}$ denotes the identity operator, and $\hat{a}^\dagger_{i\sigma}$ and $\hat{a}_{i\sigma}$ the Fermion creation and annihilation operators, respectively, associated with spatial orbital i and spin σ. Equation (12) is computed by solving the Poisson equation,

$$\nabla^2 g_{lm}(\mathbf{x}) = -4\pi\phi^*_l(\mathbf{x})\phi_m(\mathbf{x}). \tag{13}$$

It is convenient to rewrite Eq. (8) as,

$$i\dot{\phi}_i = \hat{P}\left(T\phi_i + W_i(t)\right) \tag{14}$$

where T is kinetic energy.

III. MULTI-RESOLUTION CARTESIAN GRID

We discretize spatial orbital functions on a multi-resolution Cartesian grid, inspired by the work of Bischoff and Valeev [34] and the finite volume method [35]. Figure 1 (a) schematically shows how to generate it. We start from an equidistant Cartesian grid composed of cubic cells. If a given cell is too large to represent orbital functions with sufficient accuracy, typically near the nuclei, we subdivide it into eight cubic cells with half the side length of the original cell. We continue the subdivision until accuracy requirements are satisfied. The center of each cube is taken as the grid point representing the cell.

The Laplacian $\nabla^2\phi$ of orbital function $\phi(\mathbf{r}, t)$ is evaluated at each grid point by finite difference. We first illustrate it for a one-dimensional case for simplicity in Fig. 1(b). One can evaluate the second derivative of a function $f(x)$ at grid point x_i as,

$$\frac{d^2}{dx^2}f(x_i) \approx \frac{g_i^+ - g_i^-}{\Delta x_i}, \tag{15}$$

where Δx_i is the size of cell i, and the first derivatives $g_i^\pm$ at the cell boundaries are approximated by,

$$g_i^+ \approx \frac{2[f(x_{i+1}) - f(x_i)]}{\Delta x_i + \Delta x_{i+1}}, \tag{16}$$

$$g_i^- \approx \frac{2[f(x_i) - f(x_{i-1})]}{\Delta x_i + \Delta x_{i-1}}. \tag{17}$$

We show the extension to two dimensions in Fig. 1(c). Grid points are marked by red and blue circles. In order to evaluate the second derivative with respect to the

vertical direction at the center of cell i, we need the first derivative evaluated at the cell boundary marked by the orange triangle, for which we need, in turn, the value of the function at the position marked by the star in cell $i+1$. We approximate this latter by the value $f_{i+1} \equiv f(\mathbf{r}_{i+1})$ at the grid point, i.e., the center of the cell $i+1$. Though inferior in terms of accuracy, this scheme is much more advantageous in terms of computational cost over conventional methods such as the alternating direction implicit method [36], moving least squares [37, 38], and symmetric smoothed particle hydrodynamics [39, 40].

Then, in the 3D case, we evaluate the Laplacian $\nabla^2\phi(\mathbf{r})$ as,

$$\nabla^2\phi(\mathbf{r}_a) \approx L_{aa}\phi(\mathbf{r}_a) + \sum_b{}' L_{ab}\phi(\mathbf{r}_b), \tag{18}$$

where a and b are cell indices, the primed sum is taken over the cells adjacent to the a-th cell, and,

$$L_{aa} = -\sum_b{}' L_{ab}, \tag{19}$$

$$L_{ab} = \frac{l_b^2}{l_a^2}\frac{2}{l_a+l_b}\frac{1}{l_a} \qquad (a \neq b \text{ and } l_b < l_a), \tag{20}$$

$$L_{ab} = \frac{2}{l_a+l_b}\frac{1}{l_a} \qquad (a \neq b \text{ and } l_b \geq l_a), \tag{21}$$

with l_a being the side length of the a-th cell.

IV. NUMERICAL PROCEDURE

We present the essential steps of MCTDHF simulations using multi-resolution cartesian grid as follows:

Step 1: Generation of grid and Laplacian matrix

We consider a cuboid simulation region V centered at the origin: $\{\mathbf{x} = (x, y, z) \in \mathbb{R}^2 \quad | \quad x \in [-x_L, x_L], y \in [-y_L, y_L], z \in [-z_L, z_L], x_L > 0, y_L > 0, z_L > 0\}$. We set the locations of grid points and prepare Laplacian matrix elements L_{ab} using Eqs. (19)–(21). These are done only once in the beginning.

Step 2: Computation of ρ and $\rho^{(2)}$

Each time step starts with computation of ρ and $\rho^{(2)}$, using Eqs. (10) and (11), respectively.

Step 3: Computation of g_{lm}

We solve the Poisson equation (13) to obtain g_{lm}, by the conjugate residual method [41, 42]. The condition at the simulation boundary ∂V is given by multipole expansion

$$g_{lm}(\mathbf{x}_{\rm bound}) = \int_V \frac{1}{|\mathbf{x}_{\rm bound} - \mathbf{x}'|}\phi_l^*(\mathbf{x}')\phi_m^*(\mathbf{x}')d\mathbf{x}' \tag{22}$$

$$= \sum_{l=0}^{\infty}\int_V \frac{|\mathbf{x}'|^l P_l(\cos\theta)}{|\mathbf{x}_{\rm bound}|^{l+1}}\phi_l^*(\mathbf{x}')\phi_m^*(\mathbf{x}')d\mathbf{x}' \tag{23}$$

for $\mathbf{x}_{\rm bound} \in \partial V$ where $P_l(z)$ denotes the Legendre polynomial, and θ the angle between $\mathbf{x}'$ and $\mathbf{x}_{\rm bound}$. In the present study, we truncate the sum in Eq. (23) at $l = 2$ (second-order multipole expansion).

Step 4: Time propagation of c_J and ϕ_i

We solve the equations of motion Eqs. (7) and (14) using a second-order exponential integrator [43, 44]. Equation (7) is integrated as,

$$c_J^{(1)}(t+\Delta t) = c_J(t) + \Delta t\sum_K \langle J|H|K\rangle c_K, \tag{24}$$

$$c_J^{(2)}(t+\Delta t) = c_J^{(1)}(t+\Delta t) + \Delta t\sum_K \langle J^{(1)}|H|K^{(1)}\rangle c_K^{(1)}(t+\Delta t), \tag{25}$$

$$c_J(t+\Delta t) = \frac{c_J(t) + c_J^{(2)}(t+\Delta t)}{2}, \tag{26}$$

where $|J^{(1)}\rangle$ with superscript "(1)" denotes the Slater determinant constructed with orbital functions $\phi_i^{(1)}$ defined below in Eq. (27). Equation (14) is integrated as,

$$\phi_i^{(1)} = \phi_i(t) + \hat{P}\frac{1}{1+i\Delta tT/2}\left[(-i\Delta tT)\phi_i(t) + \Delta t W_i(t)\right], \tag{27}$$

$$\phi_i^{(2)}(t+\Delta t) = \phi_i^{(1)} + \hat{P}^{(1)}\frac{1}{1+i\Delta tT/2}\left[(-i\Delta tT)\phi_i^{(1)} + \Delta t W_i(t+\Delta t)\right], \tag{28}$$

$$\hat{P}^{(1)} = \hat{\mathbf{1}} - \sum_{j=1}^{M}|\phi_j^{(1)}\rangle\langle\phi_j^{(1)}|, \tag{29}$$

$$\phi_i(t+\Delta t) = \frac{\phi_i^{(2)}(t+\Delta t) + \phi_i(t)}{2}. \tag{30}$$

In Eqs. (27) and (28), $(1+i\Delta tT/2)^{-1}$ is operated by the conjugate residual method [41, 42].

Step 5a: Absorbing boundary (only in real time propagation)

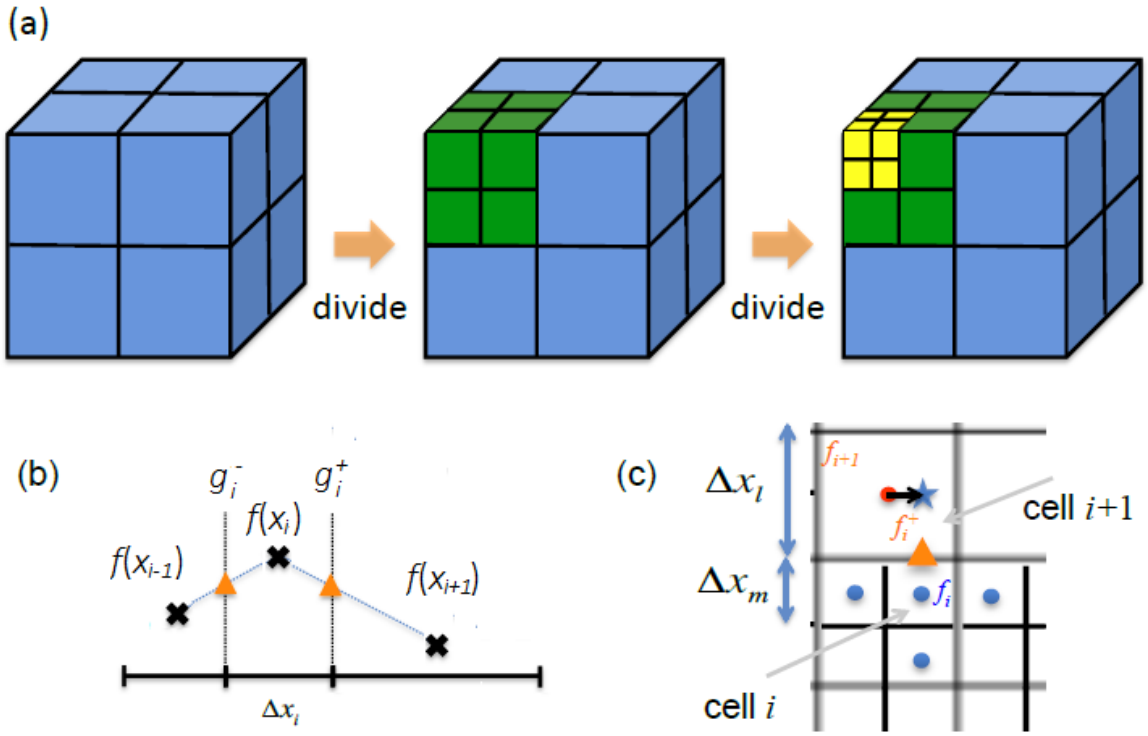

FIG. 1. (a) Schematic of the cartesian-based multi-resolution grids. (b) Schematic of the computation of second order differential at one-dimensional irregular grids. (c) Schematic of the computation of the first differential at the surface of the grid at two-dimensional irregular grids. Real grid points are red and blue circles.

To prevent the reflection from the grid boundaries, after each time step, ϕ_i is multipled by a cos mask function $M(x, y, z)$ that varies from 1 to 0 between the absorption boundary set at $x = x_0$, $y = y_0$, and $z = z_0$ $(0 < x_0 < x_L, 0 < y_0 < y_L, 0 < z_0 < z_L)$ and the outer boundary ∂V [45, 46]:

$$M(x, y, z) = C\left(\frac{|x| - x_0}{x_L - x_0}\right) C\left(\frac{|y| - y_0}{y_L - y_0}\right) C\left(\frac{|z| - z_0}{z_L - z_0}\right) \tag{31}$$

where

$$C(x) = 1 \quad (x \le 0), \quad \cos(x) \quad (x > 0). \tag{32}$$

Alternatively, one may use, e.g., exterior complex scaling [47, 48].

Step 5b: Rescaling of c_J and orthonormalization of ϕ_i (only in imaginary time propagation)

We obtain the initial ground state via imaginary time propagation [49]. After each (imaginary) time step, c_J is rescaled so that $\sum_J |c_J|^2 = 1$, and ϕ_i is orthonormalized through the Gram-Schmidt algorithm.

Step 6: End of time step

We go back to Step 2 to start next time step.

V. EXAMPLES

A. Benchmark : HHG from helium

We simulate HHG from a helium atom located at the origin. Side length of the cell is set to be 0.6 $(r > 4)$, 0.3 $(2 < r < 4)$ and $0.15(r < 2)$ respectively, depending on the distance r of the grid point at the center of each cell and the origin. We also set $x_L = 70, y_L = z_L = 35$ and $x_0 = 0.7x_L, y_0 = 0.7y_L, z_0 = 0.7z_L$. The time step size Δt is set to be 0.0025. We consider a laser pulse linearly polarized along the x axis, whose electric field $E(t)$ is given by,

$$E(t) = E_{\rm env}(t) \sin \omega t, \tag{33}$$

$$E_{\rm env}(t) = \begin{cases} \omega t/2\pi & (\omega t < 2\pi), \\ 2 - \omega t/2\pi & (2\pi < \omega t < 4\pi), \\ 0 & (\text{otherwise}), \end{cases} \tag{34}$$

with a central wavelength of 400 nm and a peak intensity of 8×10^{14} W/cm^2. For such an ultrashort pulse, the cutoff energy predicted by the semiclassical three step model [50, 51] is $I_p + 2.07U_p = 49.6$ eV, which corresponds to the 16.0 th order where I_p is ionization potential and U_p is pondermotive energy. The harmonic spectrum is obtained from the Fourier transform of the dipole acceleration.

In Fig. 2 we compare the HHG spectrum calculated

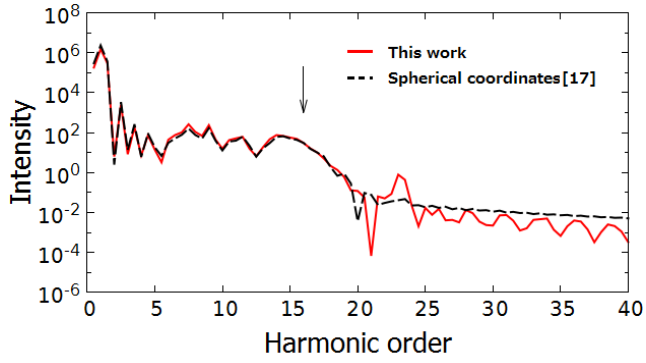

FIG. 2. HHG spectrum of helium computed by multi-resolution MCTDHF(red-solid) and method of [17](black-dashed). Arrows represent the cutoff energy.

number of	largest cell side length l_0			
orbital M	0.7	0.7*	0.6	0.55
1	-1.83661	-1.83622	-1.84318	-1.84123
2	-1.85451	-1.85467	-1.86164	-1.85964
3	-1.86218	-1.86233	-1.86925	-1.86723
6	-1.87329	-1.87342	-1.88027	-1.87756

TABLE I. Ground-state energy (a.u.) of a hydrogen molecule, obtained by relaxation in imaginary time. The values in column labeled "0.7*" are obtained with grids displaced parallel to the x axis by 0.025 a.u.

with the present implementation with that calculated with another implementation in spherical coordinates [17]. One can see that they agree with each other very well.

B. HHG from a hydrogen molecule

Next, we simulate HHG from molecular hydrogen where two hydrogen atoms are located at $(\pm 0.7, 0, 0)$, respectively. Side length of cell is set to be l_0 ($r_0 > 4$), $l_0/2$ ($2 < r_0 < 4$) and $l_0/4$($r_0 < 2$), respectively where l_0 is the side length of the largest cells (see Table I for its values). We also set $x_L = y_L = z_L = 27$ and $x_0 = 0.7x_L, y_0 = 0.7y_L, z_0 = 0.7z_L$. The time step size Δt is set to be 0.01.

The ground-state energy, obtained through relaxation in imaginary time, is shown in Table I where M is the number of orbitals. It consistently tends to the literature value -1.8884 a.u. [52] with an increasing number of orbitals. The slight dependence on M and l_0 has only a small impact on calculated harmonic spectra, as we will see below in Fig. 3(a,b). The values in column labeled "0.7*" are obtained with grids displaced parallel to the x axis by 0.025. One can see that the resulting loss of grid symmetry with respect to the yz plane also has only a small impact.

Let us consider a linearly polarized laser pulse with a central wavelength of 800 nm, a peak intensity of 1×10^{14} W/cm^2, and an eight-cycle sine-squared envelope,

$$E(t) = E_0 \sin^2(\omega t/16)\cos(\omega t). \quad (35)$$

Figure 3 presents HHG spectra for laser polarization parallel to the molecular axis (the x axis) [Fig. 3(a)(b)] and 30 degrees from the molecular axis [Fig. 3(c)]. The cutoff energy predicted by the semiclassical three step model is 34.3 eV, which corresponds to order 22.1. One can see that the simulation is converged with respect to the number of orbitals [Fig. 3(a)] and grid spacing [Fig. 3(b)]. Our multi-resolution Cartesian-grid MCTDHF, with no a priori assumption of symmetry, can also handle laser polarization oblique to the molecular axis [Fig. 3(c)].

In Fig. 3 we can clearly see the second plateau, somewhat weaker than the first one, extending beyond the cutoff ($\sim$ order 22.1). The second cutoff position is consistent with the value (53.6 eV or the 34.6-th order) predicted by the three step model with the ionization potential of H_2^+ (34.7 eV). Hence, based on a speculation that the second plateau harmonics are generated from H_2^+ produced via strong-field ionization, we have simulated HHG from this molecular ion with the same laser parameters. The obtained harmonic spectrum multiplied with the ionization probability of H_2 (2.4×10^{-4}) is plotted as a yellow dashed line in Fig. 3(a). The spectrum is much weaker than the second plateau from H_2.

Presumably, the harmonic response from H_2^+ is substantially enhanced by the action of the oscillating dipole formed by the recolliding first electron ejected from the neutral molecule and the neutral ground state. This mechanics is similar to enhancement by an assisting harmonic pulse [53–56], but the enhancement is due to direct Coulomb force from the oscillating dipole, rather than harmonics emitted from it. In the words of the semiclassical three-step model, the recolliding first electron virtually excites H_2^+, facilitating second ionization. Thus, electron-electron interaction plays an important role in high-harmonic generation in some cases, whereas HHG is usually considered as a predominantly single-electron process.

C. HHG from a water molecule

As an example of application to molecules of lower symmetry, we simulate HHG from a water molecule with its oxygen atom located at the origin and two hydrogen atoms at $(\pm 1.4299, 1.10718, 0)$. Side length of cell is set to be 0.6 ($r_0 > 4$), 0.3 ($2 < r_0 < 4$) and 0.15($r_0 < 2$) respectively where r_0 is the distance from the nearest atom. Outer boundary x_L, y_L, z_L is set to be 60 (axis parallel to the polarization) and 30 (axis parpendicular to the polarization) and absorption boundary x_0, y_0, z_0 is set to be 0.7 times as long as outer boundary. Step size Δt is set to be 0.0025. We use the same laser pulse shape as in Sec. V A. The cutoff energy predicted by the semiclassical three step model is 37.3 eV, which corresponds to the 12.0 th order.

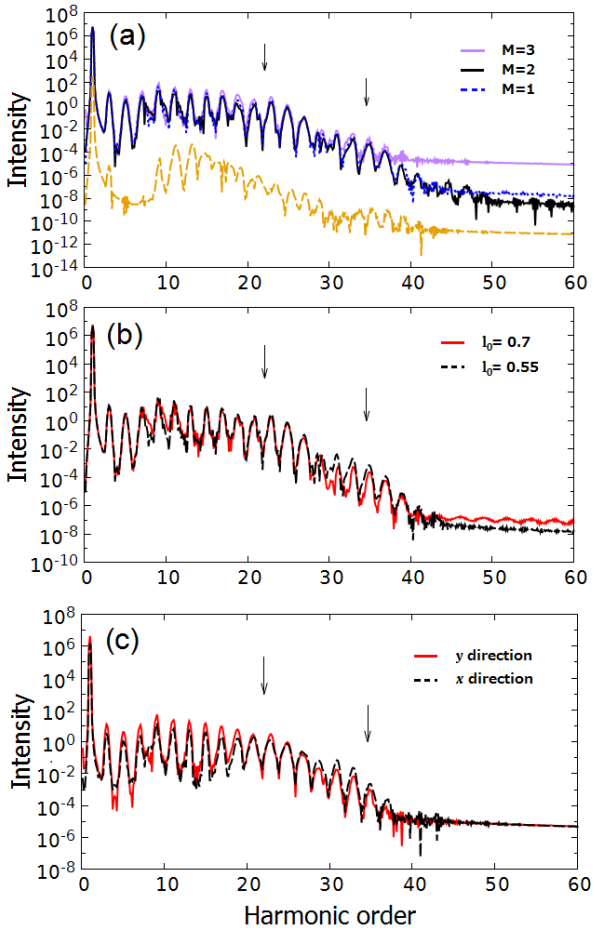

FIG. 3. Calculated high-harmonic spectra from a hydrogen molecule. See text for laser parameters. (a) Comparison of the results with $M = 1$(blue-dotted), $M = 2$ (black-solid), and $M = 3$(purple-solid), for laser polarization parallel to the molecular axis. Yellow-dashed line: spectrum from H_2^+ multiplied with the ionization probability of H_2 (2.4×10^{-4}). (b) Comparison of the results with $l_0 = 0.7$ (red-solid) and 0.55 (black-dashed). The calculation was done with $M = 1$ for polarization parallel to the molecular axis. (c) Result for laser polarization 30 degrees from the molecular axis [polarization direction is $(\cos 30°, \sin 30°, 0)$]. $M = 3$ was used. Red-solid: harmonics emitted in the y direction, black-dashed: in the x direction. Arrows in each panel indicate the cutoff positions expected for H_2 (22.1-th order) and H_2^+ (34.6-th order).

Figure 4, which presents calculated harmonic spectra for three different directions of laser polarization, demonstrates high flexibility of the multi-resolution Cartesian-grid MCTDHF implementation.

VI. CONCLUSION

We have numerically implemented the MCTDHF method on a multi-resolution Cartesian grid. Whereas previous approaches have relied on underlying symmetries of simulated atoms and molecules, the present implementation offers a flexible framework to describe strong-field and attosecond processes of real general molecules. Extension to computationally more compact methods such as TD-CASSCF [8] and TD-ORMAS [9] will be rather straightforward and enable application to large molecules.

As demonstrations, we have successfully calculated high-harmonic spectra from He, H_2, and H_2O. As the presence of the second plateau in Fig. 3 implies, the present implementation will uncover yet unexplored multi-electron, multi-channel, and multi-orbital effects, which only first-principles simulations can reveal.

ACKNOWLEDGMENTS

This work was supported in part by JSPS KAKENHI Grant Numbers 25286064, 26390076, 26600111, and 26-10100. This research was also partially supported by the Photon Frontier Network Program of the Ministry of Education, Culture, Sports, Science and Technology (MEXT) of Japan, the Advanced Integration Science Innovation Education and Research Consortium Program of MEXT, the Center of Innovation Program from Japan Science and Technology Agency (JST), and CREST, JST. R.S. gratefully acknowledges support by Graduate School of Engineering, the University of Tokyo Doctoral Student Special Incentives Program (SEUT Fellowship).

[1] F. Krausz and M. Ivanov, Rev. Mod. Phys. **81**, 163 (2009).
[2] R. Levis, G. Menkir, and H. Rabitz, Science **292**, 709 (2001).
[3] F. Calegari, D. Ayuso, A. Trabattoni, L. Belshaw, S. D. Camillis, S. Anumula, F. Frassetto, L. Poletto, A. Palacios, P. Decleva, J. B. Greenwood, F. Martín, and M. Nisoli, Science **346**, 336 (2014).
[4] K. Ishikawa and T. Sato, IEEE J. Sel. Topics Quantum Electron. **21**, 8700916 (2015).
[5] T.-T. Nguyen-Dang, M. Peters, S.-M. Wang, and F. Dion, Chem. Phys. **366**, 71 (2009).
[6] T.-T. Nguyen-Dang and J. Viau-Trudel, J. Chem. Phys. **139**, 244102 (2013).
[7] R. P. Miranda, A. J. Fisher, L. Stella, and A. P. Horsfield, J. Chem. Phys. **134**, 244101 (2011).
[8] T. Sato and K. L. Ishikawa, Phys. Rev. A **88**, 023402 (2013).
[9] T. Sato and K. L. Ishikawa, Phys. Rev. A **91**, 023417 (2015).
[10] L. Greenman, P. J. Ho, S. Pabst, E. Kamarchik, D. A. Mazziotti, and R. Santra, Phys. Rev. A **82**, 023406

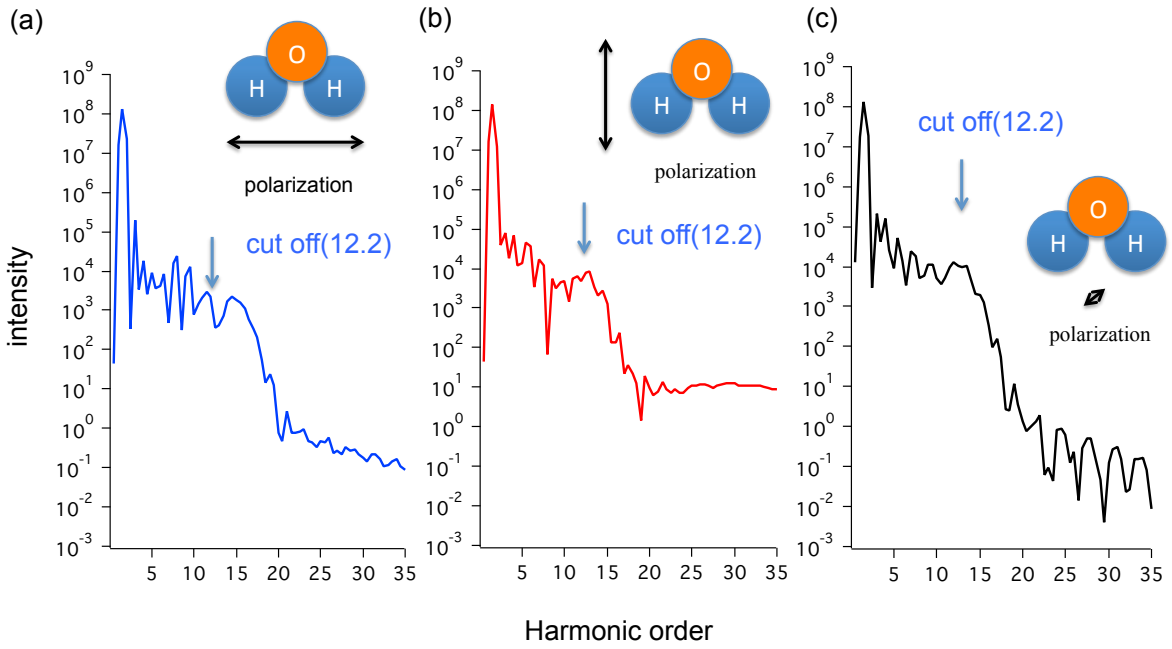

FIG. 4. High-harmonic spectra from a water molecule, calculated with $M = 6$, for three different directions of laser polarization indicated in each panel. Laser polarization in (c) is perpendicular to the plane of the molecule. See text for laser parameters.

(2010).

[11] S. Bauch, L. K. S. rensen, and L. B. Madsen, Phys. Rev. **90**, 062508 (2014).

[12] J. Caillat, J. Zanghellini, M. Kitzler, O. Koch, W. Kreuzer, and A. Scrinzi, Phys. Rev. A **71**, 012712 (2005).

[13] T. Kato and H. Kono, Chem. Phys. Lett. **392**, 533 (2004).

[14] D. J. Haxton and C. W. McCurdy, Phys. Rev. A **91**, 012509 (2015).

[15] H. Miyagi and L. B. Madsen, Phys. Rev. A **87**, 062511 (2013).

[16] D. J. Haxton, K. V. Lawler, and C. W. McCurdy, Phys. Rev. A **86**, 013406 (2012).

[17] T. Sato and K. L. Ishikawa, Unpublished.

[18] J. Parker, K. T. Taylor, C. W. Clark, and S. Blodgett-Ford, Journal of Physics B: Atomic, Molecular and Optical Physics **29**, L33 (1996).

[19] E. S. Smyth, J. S. Parker, and K. Taylor, Comput. Phys. Commun. **114**, 1 (1998).

[20] K. L. Ishikawa and K. Midorikawa, Phys. Rev. A **72**, 013407 (2005).

[21] K. L. Ishikawa and K. Ueda, Phys. Rev. Lett. **108**, 033003 (2012).

[22] K. L. Ishikawa and K. Ueda, Appl. Sci. **3**, 189 (2013).

[23] K. Harumiya, I. Kawata, H. Kono, and Y. Fujimura, J. Chem. Phys. **113**, 8953 (2000).

[24] K. Harumiya, H. Kono, Y. Fujimura, I. Kawata, and A. D. Bandrauk, Phys. Rev. A **66**, 043403 (2002).

[25] S. Ohmura, T. Oyamada, T. Kato, H. Kono, and S. Koseki, eds., *Molecular Orbital Analysis of High Harmonic Generation*, Vol. 1 (Asia Pacific Physics Conference, 2014).

[26] S. Ohmura, H. Kono, T. Oyamada, T. Kato, K. Nakai, and S. Koseki, J. Chem. Phys. **141**, 114105 (2014).

[27] X. Guan, K. Bartschat, and B. I. Schneider, Phys. Rev. A **82**, 041404 (2010).

[28] L. Tao, C. W. McCurdy, and T. N. Rescigno, Phys. Rev. A **79**, 012719 (2009).

[29] L. Tao, C. W. McCurdy, and T. N. Rescigno, Phys. Rev. A **80**, 013402 (2009).

[30] L. Tao, C. W. McCurdy, and T. N. Rescigno, Phys. Rev. A **82**, 023423 (2010).

[31] P. A. M. Dirac, Proc. Cambridge Phil. Roy. Soc. **26**, 376 (1930).

[32] J.Frenkel, *Wave Mechanics. Advanced General Theory.*, edited by C. Press (Clarendon Press, 1934).

[33] P. Kramer and M. Saraceno, *Geometry of the Time-Dependent Variational Principle*, edited by Springer (Springer, 1981).

[34] F. A. Bischoff and E. F. Valeev, J. Chem. Phys. **134**, 104104 (2011).

[35] H. Versteeg and W. Malalasekera, *An Introduction to Computational Fluid Dynamics: The Finite Volume Method* (Prentice Hall, 2007).

[36] D. W. Peaceman and J. H. H. Rachford, Journal of the Society for Industrial and Applied Mathematics **3**, 28 (1955).

[37] D. Levin, Mathematics of Computation **67**, 1517 (1998).

[38] C. L. Lopreore and R. E. Wyatt, Phys. Rev. Lett. **82**, 5190 (1999).

[39] R. C. Batra and G. M. Zhang, Computational Mechanics **41**, 527 (2008).

[40] C. L. Tsai, Y. L. Guan, R. C. Batra, D. C. Ohanehi, J. G. Dillard, E. Nicoli, and D. A. Dillard, Computational Mechanics **51**, 19 (2013).

[41] E. Steiefel, Commentarii Mathematici Helvetici **29**, 157 (1955).

[42] Y. Saad, *Iterative Methods for Sparse Linear Systems*, edited by S. for Industrial and A. Mathematics (Society for Industrial and Applied Mathematics, 2003).

[43] S. Cox and P. Matthews, Journal of Computational Physics **176**, 430 (2002).
[44] A. Bandrauk and H. Lu, Journal of Theoretical & Computational Chemistry **12**, 1340001 (2013).
[45] J. L. Krause, K. J. Schafer, and K. C. Kulander, Phys. Rev. A **45**, 4998 (1992).
[46] M. Beck, A. Jäckle, G. Worth, and H.-D. Meyer, Physical Reports **324**, 1 (2000).
[47] A. Scrinzi and B. Piraux, Phys. Rev. A **58**, 1310 (1998).
[48] A. Scrinzi, Phys. Rev. A **81**, 053845 (2010).
[49] R. Kosloff and H. Tal-Ezer, Chem. Phys. Lett. **127**, 223 (1986).
[50] P. B. Corkum, Phys. Rev. Lett. **71**, 1994 (1993).
[51] J. L. K. K.C. Kulander, K.J. Schafer, in *Super-Intense Laser-Atom Physics*, NATO ASI, Ser. B, Vol. 316, edited by B. Piraux, A. L'Huillier, and K. Rzążewski (Plenum Press, New York, 1993) p. 95.
[52] A. Turbiner and N. Guevara, arXiv [atom-ph] , 0606120 (2007).
[53] K. Ishikawa, Phys. Rev. Lett. **91**, 043002 (2003).
[54] K. L. Ishikawa, Phys. Rev. A **70**, 013412 (2004).
[55] E. J. Takahashi, T. Kanai, K. L. Ishikawa, Y. Nabekawa, and K. Midorikawa, Phys. Rev. Lett. **99**, 053904 (2007).
[56] K. L. Ishikawa, E. J. Takahashi, and K. Midorikawa, Phys. Rev. A **80**, 011807 (2009).